Journal of Energy Chemistry 77 (2023) 529–534

Contents lists available at ScienceDirect

Journal of Energy Chemistry

journal homepage: www.elsevier.com/locate/jechem

http://www.journals.elsevier.com/journal-of-energy-chemistry/

Spectroscopic characterization of chain-to-ring structural evolution in platinum carbide clusters

Yu Zhang [a,b,1], Shihu Du [a,c,1], Zhi Zhao [c], Haiyan Han [c], Gang Li [a], Jinghan Zou [a], Hua Xie [a,*], Ling Jiang [a,*]

[a] State Key Laboratory of Molecular Reaction Dynamics, Dalian Institute of Chemical Physics, Chinese Academy of Sciences, Dalian 116023, Liaoning, China
[b] College of Chemistry and Chemical Engineering, Xinyang Normal University, Xinyang 464000, Henan, China
[c] School of Mathematics and Physics, Hebei University of Engineering, Handan 056038, Hebei, China

ARTICLE INFO

Article history:
Received 28 October 2022
Revised 14 November 2022
Accepted 19 November 2022
Available online 25 November 2022

Keywords:
Catalysis
Functional material
Metal carbide
Photoelectron velocity-map imaging spectroscopy
Quantum chemical calculation

ABSTRACT

Metal carbides play an important role in catalysis and functional materials. However, the structural characterization of metal carbide clusters has been proven to be a challenging experimental target due to the difficulty in size selection. Here we use the size-specific photoelectron velocity-map imaging spectroscopy to study the structures and properties of platinum carbide clusters. Quantum chemical calculations are carried out to identify the structures and to assign the experimental spectra. The results indicate that the cluster size of the chain-to-ring structural evolution for the PtC_n^- anions occurs at n = 14, whereas that for the PtC_n neutrals at n = 10, revealing a significant effect of charge on the structures of metal carbides. The greatest importance of these building blocks is the strong preference of the Pt atom to expose in the outer side of the chain or ring, exhibiting the active sites for catalyzing potential reactions. These findings provide unique spectroscopic snapshots for the formation and growth of platinum carbide clusters and have important implications in the development of related single-atom catalysts with isolated metal atoms dispersed on supports.

1. Introduction

Metal carbides play an important role in various industrial applications due to their excellent chemical and physical properties, such as noble-metal-like catalytic activity, high electrical conductivity, high thermal conductivity, high energy storage performance, high melting point, and high hardness [1–3]. With these peculiar features, they are receiving increasing attentions, especially in the fields of catalysis and functional materials. The combination of transition metals and carbon atoms was proposed to form exotic structures such as endohedral metallofullerenes [4,5] and metallocarbohedrenes (Met-Cars) [6–9]. Metal carbides with two-dimensional structures can also be prepared and utilized as electrode materials for supercapacitors and batteries [10–12]. Thus, elucidating the interplays between the metals and carbon atoms is crucial to understanding the structure–reactivity relationship and the mechanism of single-atom catalysts with isolated metal atoms dispersed on supports [13–15].

Spectroscopic studies of metal carbide clusters under well-defined conditions help uncover the relationship between the structure and function at the molecular level which is difficult to extract from the condensed-phase experiments. Experimental and theoretical efforts have been made to study the metal carbide clusters in recent decades [16–19]. Wang and coworkers investigated the structures and electronic properties of small-sized clusters MC_n^- (M = Fe, Ti, Cr, Nb) [9,20–25] and $Al_mC_n^-$ clusters [26–29] with the aid of photoelectron spectroscopy (PES). Using the same experimental approach in conjunction with quantum chemical calculations, Zheng et al. examined the $Co_mC_n^-$ [30,31], $Al_mC_n^-$ [32,33], and $V_mC_n^-$ clusters [34].

Recent studies reveal that platinum carbide nanomaterials exhibit remarkably higher activity in catalytic hydrocarbon conversion than platinum nanoparticles [35]. Although the structures of some platinum carbide compounds have been investigated both experimentally and theoretically [36–41], the systematical study of platinum carbide clusters remains rare. Herein, we report a study on the geometric structures and electronic properties of a series of platinum carbide clusters by using photoelectron velocity map imaging spectroscopy and density functional theory calculations. Experimental and theoretical results reveal that the structural evolution of the anionic PtC_n^- clusters from the chain into

* Corresponding authors.
E-mail addresses: xiehua@dicp.ac.cn (H. Xie), ljiang@dicp.ac.cn (L. Jiang).
[1] These authors contributed equally to this work.

https://doi.org/10.1016/j.jechem.2022.11.033

ring structure occurs at n = 14 and the charge has a significant effect on the structures of metal carbides.

2. Methods

2.1. Experimental method

The experiments were performed by using a homemade photoelectron imaging spectrometer, coupled with a laser ablation supersonic cluster source and a dual-channel time-of-flight mass spectrometer [42,43]. The PtC_n^- clusters were generated via laser ablation of a platinum–carbon mixture target (mole ratio, Pt/C = 1:4) under the supersonic expansion of pulsed high-pressure helium carrier gas. The cluster anions were transferred into the extraction area of the first-stage TOF-MS and mass-selected, before being interacted with a laser beam of 266 nm (4.661 eV). The photoelectrons were captured by the velocity-map imaging photoelectron spectrometer and recorded by a charge-coupled device (CCD) camera. Each raw 2D image was collected by gathering 10000–50000 laser shots at a repetition rate of 10 Hz and subsequently reconstructed by using the Basis Set Expansion (BASEX) inverse Abel transform method [44]. The photoelectron spectra were acquired by integrating the central slice of each reconstructed 3D image. The photoelectron spectra were calibrated with the known spectrum of Au^-, showing an energy resolution better than 5 % (50 meV at an electron kinetic energy of 1 eV).

2.2. Computational method

To elucidate the geometrical and electronic structures of PtC_n^-, theoretical calculations were performed with the Gaussian 09 program [45]. The structures were optimized using the B3LYP functional together with the basis set of 6–311 + G* for C atoms, and SDD for Pt atom (hereafter referred to as the B3LYP/6–311 + G*/SDD level of theory) [46]. The stability of the wave function has been checked. The possible electronic states of anionic and neutral structures have been calculated. Harmonic frequency analysis was carried out to ensure that the located structures were real minima on the potential energy surfaces and to obtain the zero-point energy (ZPE) corrections. Theoretically, the vertical detachment energy (VDE) was calculated as the energy difference between the neutral and anion based on the optimized geometry of the anion, while the adiabatic detachment energy (ADE) was determined as the energy difference between the neutral and anion at each of their optimized geometries with the ZPE corrections.

3. Results

The experimental photoelectron imaging spectra of PtC_n^- (n = 7–16) recorded at 266 nm (4.661 eV) are shown in Fig. 1, in which the images in purple background denote the central slice of the 3D lab frame photoelectron distribution reconstructed from the original 2D projection. The electron binding energy (EBE) of the maximum of each dominant band (labeled with X) corresponds to the VDE of the ground state, which can be directly measured to be 3.13, 3.99, 3.36, 3.88, 3.90, 3.80, 3.96, 4.11, 4.18, and 4.06 eV for n = 7–16 (Table 1), respectively. The extra band (labeled X') appears in the n = 11, 13, and 15 spectra, implying the presence of low-lying isomers. The lack of vibrational details and the indiscernible 0–0 bands prevent us from directly gauging the ground-state adiabatic detachment energies (ADEs), which can be alternatively estimated by the intersection of a straight line drawn along the rising edge of the X band, together with the instrumental resolution. The ADE values of the X bands for PtC_n^- (n = 7–16) are evaluated to be 2.89, 3.76, 3.27, 3.43, 3.70, 3.39, 3.70, 3.71, 3.73, 3.65 eV (Table 1), respectively.

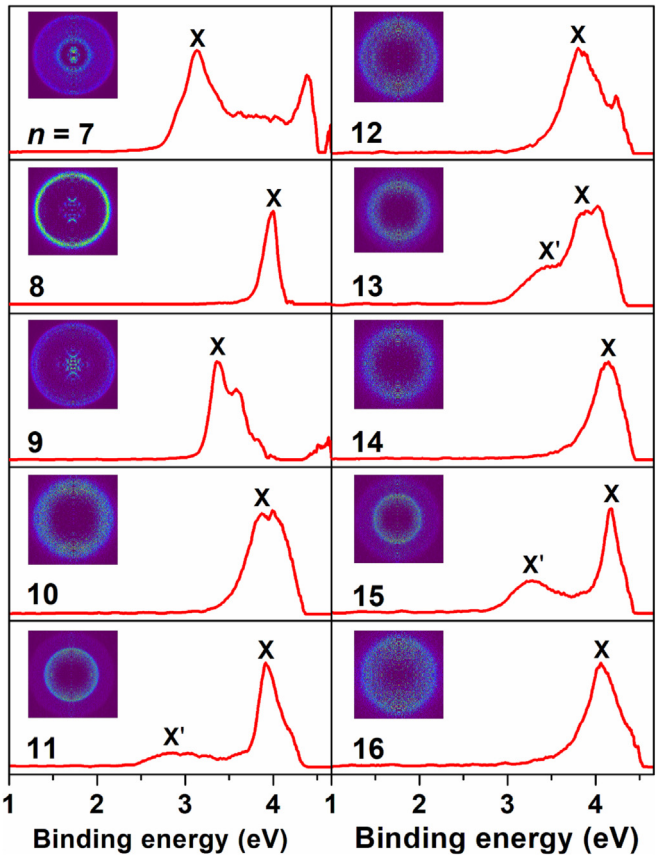

Fig. 1. Photoelectron spectra of PtC_n^- (n = 7–16) at 266 nm (4.661 eV). Photoelectron images after inverse Abel transformation are embedded in the photoelectron spectra.

In order to assign the observed spectral features and to determine the structures of the low-lying isomers, quantum chemical calculations at the B3LYP/6–311 + G*/SDD level of theory have been performed for the PtC_n^- anions and the PtC_n neutrals (n = 7–16). The optimized structures of the three lowest-energy isomers (labeled as nA-nC) for the PtC_n^- anions are shown in Fig. 2. Other low-lying isomers and the neutral counterparts are illustrated in Fig. S2 and Fig. S3, respectively. The theoretical VDEs and ADEs of the nA-nC isomers are summarized in Table 1 to compare with the experimentally measured values. The densities of states (DOS) spectra of the nA-nC isomers were simulated on the basis of the theoretically generalized Koopman's theorem and are compared with the experimental spectra in Fig. 3 and Fig. 4.

3.1. PtC_7^-

For PtC_7^-, the lowest-lying isomer (7A) exhibits a $C_{\infty v}$ symmetric linear chain structure with a $^2\Sigma^+$ electronic state (Fig. 2). Isomer 7B is 0.92 eV higher in energy than isomer 7A, showing a C_s symmetric and completely closed cyclic structure with a ^{2}A' electronic state. Isomer 7C lies 0.98 eV higher in energy than isomer 7A and possesses C_{2v} symmetry with an electronic state of $^2A_1$. Isomer 7C presents a chain geometry with a special carbon triangle located at the end away from the Pt atom.

The calculated VDE and ADE values of 7A (3.12 and 2.98 eV) agree well with the experimental values (3.13 and 2.89 eV) (Table 1). While the calculated VDE and ADE values of 7B (2.77 and 2.28 eV) are obviously lower than the experimental values, those of 7C (3.70 and 3.51 eV) are much higher than the experimental ones. As

Table 1
Comparison of experimental and calculated VDE and ADE values of the three lowest-energy isomers for PtC_n^- (n = 7–16).

Cluster	Isomer	VDE		ADE	
		Expt.[a]	Calc.	Expt.[a]	Calc.
n = 7	7A	3.13(8)	3.12	2.89(9)	2.98
	7B		2.77		2.28
	7C		3.70		3.51
n = 8	8A	3.99(3)	3.97	3.76(5)	3.83
	8B		3.22		2.98
	8C		3.89		3.78
n = 9	9A	3.36(7)	3.43	3.27(7)	3.32
	9B		3.91		3.75
	9C		3.46		3.01
n = 10	10A	3.88(4)	4.03	3.43(6)	3.47
	10B		3.76		3.64
	10C		3.47		3.34
n = 11	11A	3.90(4)	3.87	3.70(5)	3.66
	11B	2.87(9)	2.88	2.62(10)	2.69
	11C		4.08		3.69
n = 12	12A	3.80(4)	3.85	3.39(6)	3.34
	12B		3.51		3.29
	12C		4.17		3.80
n = 13	13A	3.96(4)	4.00	3.70(5)	3.78
	13B	3.43(6)	3.46	3.16(8)	3.10
	13C		3.65		3.36
n = 14	14A	4.11(3)	4.03	3.71(5)	3.85
	14B		4.35		4.23
	14C		3.48		3.25
n = 15	15A	3.16(7)	3.18	2.85(9)	3.08
	15B	4.18(4)	4.00	3.73(6)	3.80
	15C		3.35		3.72
n = 16	16A	4.06(3)	4.02	3.65(5)	3.55
	16B		4.44		4.29
	16C		3.41		3.33

[a] Numbers in parentheses are experimental uncertainties in the last digit. The energy resolution was better than 50 meV at electron kinetic energy (eKE) of 1 eV (5 %). The experimental ADE and VDE error bars were determined by the energy resolution at the corresponding ekE.

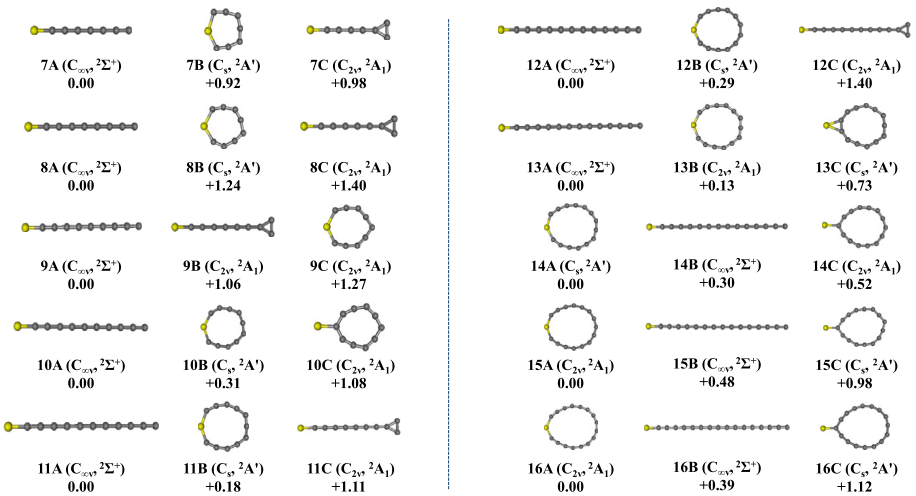

Fig. 2. Optimized structures of the three lowest-energy isomers of PtC_n^- (n = 7–16) calculated at the B3LYP/6–311 + G*/SDD level of theory (Pt, yellow; carbon, gray). Relative energies are given in eV.

shown in Fig. 3, the simulated spectrum of isomer 7A agrees best with the experimental one, confirming the assignment of isomer 7A to be responsible for the experimental spectrum. It thus appears that the presence of isomers 7B and 7C can be ruled out.

3.2. PtC_8^-

For PtC_8^-, the most stable isomer (8A) is characterized by a $C_{\infty v}$ symmetric linear geometry with a $^2\Sigma^+$ ground state. Isomers 8B and 8C exhibit similar structures to the 7B and 7C, respectively. As listed in Table 1, the calculated VDE and ADE values of isomer 8A are 3.97 and 3.83 eV, respectively, which are in excellent agreement with the experimental results (3.99 and 3.76 eV). The calculated VDE and ADE values of isomer 8B (3.22 and 2.98 eV) are remarkably lower than the experimental values. Although the calculated VDE and ADE values of isomer 8C (3.89 and 3.78 eV) are close to the experimental values, isomer 8C should be too high in energy to be probed in the experiment. Moreover, the simulated spectrum of 8A well reproduces the experimental spectrum (Fig. 3). The disagreement between the simulated spectra of isomers 8B and 8C with the experimental spectrum excludes their contributions.

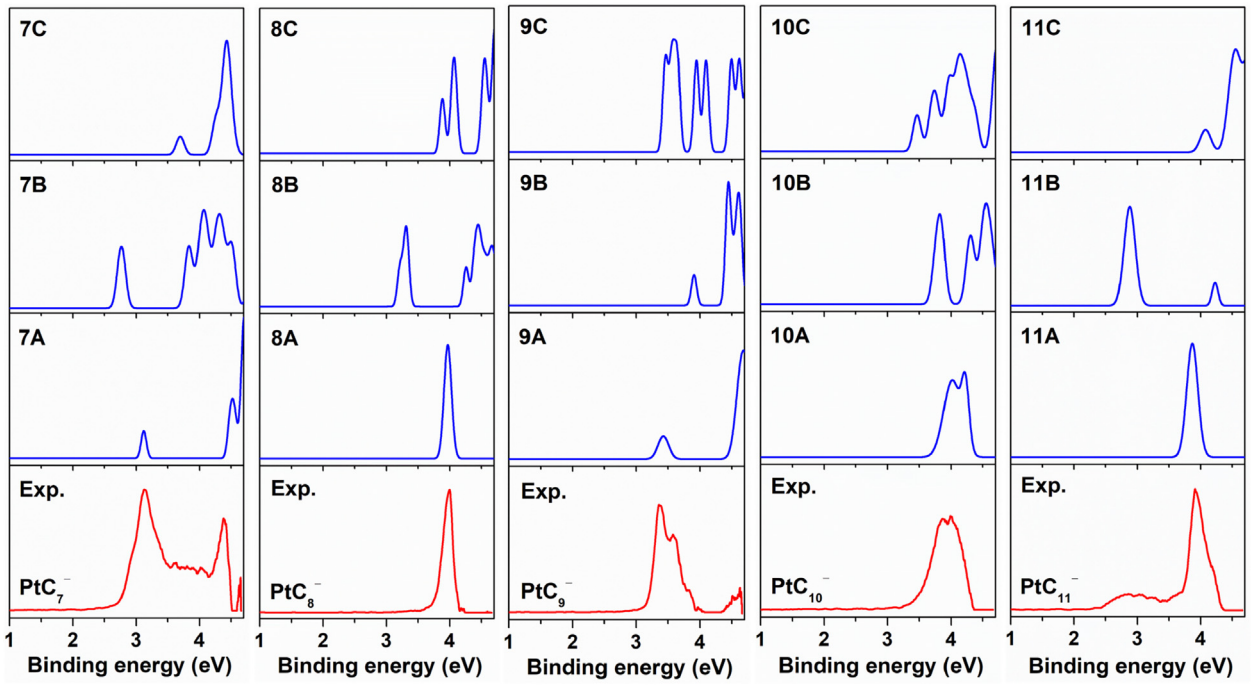

Fig. 3. Comparison of experimental 266 nm photoelectron spectra (bottom rows) of PtC_n^- (n = 7–11) to the simulated spectra of the three lowest-energy isomers (top rows).

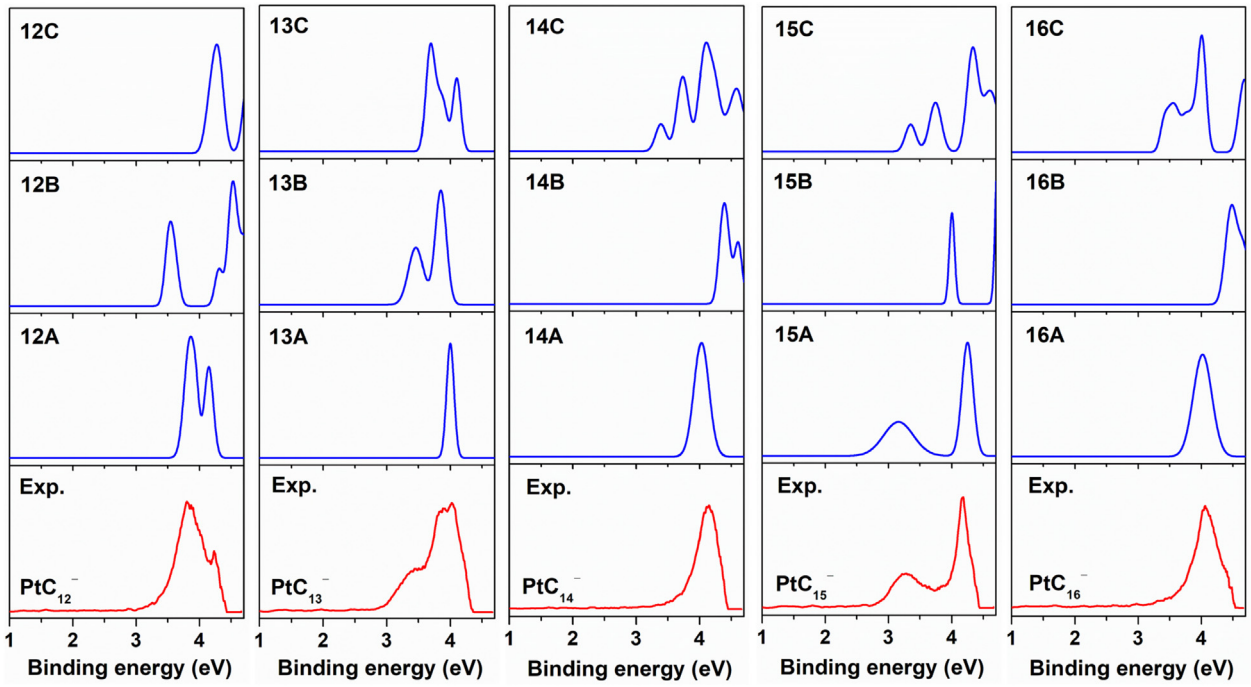

Fig. 4. Comparison of experimental 266 nm photoelectron spectra (bottom rows) of PtC_n^- (n = 12–16) to the simulated spectra of the three lowest-energy isomers (top rows).

3.3. PtC_n^- (n = 9–13)

The structure of the lowest-lying isomer of each cluster of PtC_n^- (n = 9–13) (9A-13A) is similar to that of isomers 7A and 8A. The nA (n = 7–13) isomers exhibit a linear chain structure and are identified as the dominant contributors to the experimental spectra based on a comprehensive consideration of the simulated ADE/VDE values and spectral profiles (Table 1 and Fig. 3 and Fig. 4).

For the n = 11 cluster, the 11B isomer lies higher in energy than 11A by only 0.18 eV. The calculated VDE and ADE values of isomer 11B (2.88 and 2.69 eV) agree well with the experimental values of the X' band (2.87 and 2.62 eV). As shown in Fig. 3, the best agreement between the simulated and experimental spectra is obtained when assuming the mixture of isomers 11A and 11B, implying the coexistence of these two isomers. A similar result obtained for the n = 13 cluster suggests the multiple coexisting structures of chain and ring isomers.

3.4. PtC_n^- (n = 14–16)

As shown in Fig. 2, the lowest-energy isomer of each cluster of PtC_n^- (n = 14–16) (labeled 14A-16A) consists of a ring structure.

The chain structures (14B-16B) lie higher in energy than the global-minimum structures by about 0.30–0.50 kcal/mol. The calculated VDE and ADE values of isomers 14A-16A are consistent with the corresponding experimental values (Table 1), respectively. The agreement between the simulated and experimental spectra (Fig. 4) is reasonable to confirm the assignment of isomers 14A-16A to be the main structures present in the experiment.

4. Discussion

The agreement between the calculated and experimental results allows for establishing the structural evolution of platinum carbide clusters. For the PtC_n^- ($n \leq 13$) clusters, all the most stable isomers have linear chain-shaped structures. The chain-to-ring structural evolution of the anionic PtC_n^- clusters occurs at n = 14. Interestingly, the Pt atoms are preferentially bound to the outer side of both the chain and ring structures, exposing the active sites for catalyzing potential reactions [13].

As shown in Fig. S3, the most stable structures of the neutral PtC_n (n = 7–9) clusters exhibit a $C_{\infty v}$ symmetric chain structure with a $^1\Sigma^+$ electronic state. The neutral PtC_{10} cluster prefers to have a bicyclic structure that consists of a ten-carbon ring and an outer Pt atom simultaneously connecting two adjacent carbon atoms. A single cyclic structure is favorably formed in the neutral PtC_{11} and PtC_{12} clusters. Thus, the chain-to-ring structural evolution of the PtC_n neutrals occurs at n = 10, showing a smaller cluster size than the PtC_n^- anions. Such difference between the anionic PtC_n^- and neutral PtC_n clusters implies that the charge may have a significant effect on the properties of metal carbides, which would have important implications in the context of the structure–reactivity relationship [35]. Indeed, the effect of charge on CO binding was found in rhodium carbonyls, shedding light on the origin of electronic promoter effects in catalysis in general [47]. Since the absence of a charge makes for difficult size selection and detection, the extension to characterize the structures of neutral metal carbides dominated in the practical systems is thus a challenging but important direction for future work.

5. Conclusions

A series of platinum carbide clusters have been prepared via a laser vaporization supersonic cluster source and structurally characterized by photoelectron velocity-map imaging spectroscopy and quantum chemical calculation. The binding motifs in the most stable isomers of the anionic PtC_n^- ($n \leq 13$) clusters consist of a chain structure. Starting at n = 14, a ring structure is preferentially formed. Interestingly, the chain-to-ring structural evolution of the neutral PtC_n clusters occurs at n = 10. Such difference suggests that the charge may have a significant effect on the properties of metal carbides in the context of the structure–reactivity relationship. The present findings provide key microscopic information for a systematic understanding of the formation and growth mechanism of metal carbide clusters that are responsible for the major features of the structures and properties of condensed-phase systems.

Declaration of competing interest

The authors declare that they have no known competing financial interests or personal relationships that could have appeared to influence the work reported in this paper.

Acknowledgments

The authors gratefully acknowledge the Dalian Coherent Light Source (DCLS) for support and assistance. This work was supported by the National Natural Science Foundation of China (22273101, 22103082, 22125303, 92061203, and 22288201), the Youth Innovation Promotion Association of the Chinese Academy of Sciences (CAS) (2020187), the Innovation Program for Quantum Science and Technology (2021ZD0303304), Chinese Academy of Sciences (GJJSTD20220001), Dalian Institute of Chemical Physics (DICP DCLS201702), and K. C. Wong Education Foundation (GJTD-2018-06).

Appendix A. Supplementary material

Supplementary material to this article can be found online at https://doi.org/10.1016/j.jechem.2022.11.033.

References

[1] R.B. Levy, M. Boudart, Science 181 (1973) 547–549.
[2] O. Alévêque, P.-Y. Blanchard, T. Breton, M. Dias, C. Gautier, E. Levillain, Electrochem. Commun. 16 (2012) 6–9.
[3] Q. Tang, Z. Zhou, P. Shen, J. Am. Chem. Soc. 134 (2012) 16909–16916.
[4] Y. Chai, T. Cuo, C. Jin, R.E. Haufler, L.P.F. Chibante, J. Fure, L. Wang, J.M. Alford, R. E. Smalley, J. Phys. Chem. 95 (1991) 7564–7568.
[5] D.E. Clemmer, K.B. Shelimov, M.F. Jarrold, Nature 367 (1994) 718–720.
[6] B.C. Guo, K.P. Kerns, A.W. Castleman, Science 255 (1992) 1411–1413.
[7] B.C. Guo, S. Wei, J. Purnell, S. Buzza, A.W. Castleman, Science 256 (1992) 515–516.
[8] J.S. Wgrim, M.A. Ihcan, J. Am. Chem. Soc. 115 (1993) 6958–6961.
[9] S. Li, H. Wu, L.-S. Wang, J. Am. Chem. Soc. 119 (1997) 7418–7422.
[10] M. Naguib, M. Kurtoglu, V. Presser, J. Lu, J. Niu, M. Heon, L. Hultman, Y. Gogotsi, M.W. Barsoum, Adv. Mater. 23 (2011) 4248–4253.
[11] M. Naguib, J. Come, B. Dyatkin, V. Presser, P.-L. Taberna, P. Simon, M.W. Barsoum, Y. Gogotsi, Electrochem. Commun. 16 (2012) 61–64.
[12] Y. Zhong, X. Xia, F. Shi, J. Zhan, J. Tu, H.J. Fan, Adv. Sci. 3 (2016) 1500286.
[13] B. Qiao, A. Wang, X. Yang, L.F. Allard, Z. Jiang, Y. Cui, J. Liu, J. Li, T. Zhang, Nat. Chem. 3 (2011) 634–641.
[14] Y. Li, J. Wang, S. Fan, F. Wang, Z. Shen, H. Duan, J. Xu, Y. Huang, J. Energy Chem. 53 (2021) 168–174.
[15] X. Ye, J. Ma, W. Yu, X. Pan, C. Yang, C. Wang, Q. Liu, Y. Huang, J. Energy Chem. 67 (2022) 184–192.
[16] X. Sun, J. Du, G. Jiang, Struct. Chem. 24 (2012) 1289–1295.
[17] Z.-H. Chen, Z. Xie, Eur. Phys. J. Appl. Phys. 67 (2014) 10403.
[18] X.-L. Xu, B. Yang, C.-J. Zhang, H.-G. Xu, W.-J. Zheng, J. Chem. Phys. 150 (2019).
[19] Y. Wei, J. Xu, X. Yuan, X. Zheng, Adv. Mater. Res. 652–654 (2013) 815–818.
[20] J. Fan, L.-S. Wang, J. Phys. Chem. 98 (1994) (1817) 11814–111811.
[21] J. Fan, L. Lou, L.-S. Wang, J. Chem. Phys. 102 (1995) 2701–2707.
[22] X.-B. Wang, C.-F. Ding, L.-S. Wang, J. Phys. Chem. A 101 (1997) 7699–7701.
[23] L.-S. Wang, X.-B. Wang, H. Wu, H. Cheng, J. Am. Chem. Soc. 120 (1998) 6556–6562.
[24] H.-J. Zhai, L.-S. Wang, P. Jena, G.L. Gutsev, C.W. Bauschlicher, J. Chem. Phys. 120 (2004) 8996–9008.
[25] H.-J. Zhai, S.-R. Liu, X. Li, L.-S. Wang, J. Chem. Phys. 115 (2001) 5170–5178.
[26] A.I. Boldyrev, J. Simons, X. Li, W. Chen, L.-S. Wang, J. Chem. Phys. 110 (1999) 8980–8985.
[27] A.I. Boldyrev, J. Simons, X. Li, L.-S. Wang, J. Chem. Phys. 111 (1999) 4993–4998.
[28] X. Li, L.-S. Wang, A.I. Boldyrev, J. Simons, J. Am. Chem. Soc. 121 (1999) 6033–6038.
[29] N.A. Cannon, A.I. Boldyrev, X. Li, L.-S. Wang, J. Chem. Phys. 113 (2000) 2671–2679.
[30] J.-Y. Yuan, H.-G. Xu, W.-J. Zheng, Phys. Chem. Chem. Phys. 16 (2014) 5434–5439.
[31] X.-L. Xu, J.-Y. Yuan, B. Yang, H.-G. Xu, W.-J. Zheng, Chin. J. Chem. Phys. 30 (2017) 717–726.
[32] C.-J. Zhang, H.-G. Xu, X.-L. Xu, W.-J. Zheng, J. Phys. Chem. A 125 (2021) 302–307.
[33] C.-J. Zhang, P. Wang, X.-L. Xu, H.-G. Xu, W.-J. Zheng, Phys. Chem. Chem. Phys. 23 (2021) 1967–1975.
[34] J. Yuan, P. Wang, G.-L. Hou, G. Feng, W.-J. Zhang, X.-L. Xu, H.-G. Xu, J. Yang, W.-J. Zheng, J. Phys. Chem. A 120 (2016) 1520–1528.
[35] J. Shan, H. Wang, P. Yoo, L. Nguyen, F.-K. Chiang, S. Lee, P. Liao, J. Cheng, A.C.S. Mater. Lett. 3 (2020) 179–186.
[36] D.M. Bittner, D.P. Zaleski, D.P. Tew, N.R. Walker, A.C. Legon, Angew. Chem. Int. Ed. 55 (2016) 3768–3771.
[37] S.-J. Lu, Chem. Phys. Lett. 699 (2018) 218–222.
[38] S.-J. Lu, Chem. Phys. Lett. 694 (2018) 70–74.
[39] S.-J. Lu, X.-L. Xu, H.-G. Xu, W.-J. Zheng, J. Chem. Phys. 151 (2019).
[40] X. Liu, G. Li, Z. Liu, J. Zou, D. Yang, S. Du, W. Yang, L. Jiang, H. Xie, J. Chem. Phys. 156 (2022).
[41] X. Liu, G. Li, Z. Liu, W. Yang, H. Fan, L. Jiang, H. Xie, J. Phys. Chem. Lett. 13 (2022) 12–17.
[42] Z. Qin, X. Wu, Z. Tang, Rev. Sci. Instrum. 84 (2013).
[43] J. Zhang, Z. Liu, G. Li, H. Fan, L. Jiang, H. Xie, J. Energy Chem. 63 (2021) 344–350.

[44] V. Dribinski, A. Ossadtchi, V.A. Mandelshtam, H. Reisler, Rev. Sci. Instrum. 73 (2002) 2634–2642.
[45] M.J. Frisch, G.W. Trucks, H.B. Schlegel, G.E. Scuseria, M.A. Robb, J.R. Cheeseman, G. Scalmani, V. Barone, B. Mennucci, G.A. Petersson, H. Nakatsuji, M. Caricato, X. Li, H.P. Hratchian, A.F. Izmaylov, J. Bloino, G. Zheng, J.L. Sonnenberg, M. Hada, M. Ehara, K. Toyota, R. Fukuda, J. Hasegawa, M. Ishida, T. Nakajima, Y. Honda, O. Kitao, H. Nakai, T. Vreven, J.A. Montgomery Jr., J.E. Peralta, F. Ogliaro, M.J. Bearpark, J. Heyd, E.N. Brothers, K.N. Kudin, V.N. Staroverov, R. Kobayashi, J. Normand, K. Raghavachari, A.P. Rendell, J.C. Burant, S.S. Iyengar, J. Tomasi, M. Cossi, N. Rega, N.J. Millam, M. Klene, J.E. Knox, J.B. Cross, V. Bakken, C. Adamo, J. Jaramillo, R. Gomperts, R.E. Stratmann, O. Yazyev, A.J. Austin, R. Cammi, C. Pomelli, J.W. Ochterski, R.L. Martin, K. Morokuma, V.G. Zakrzewski, G.A. Voth, P. Salvador, J.J. Dannenberg, S. Dapprich, A.D. Daniels, O. Farkas, J.B. Foresman, J.V. Ortiz, J. Cioslowski, D, J. Fox, Gaussian Inc, Wallingford, CT, USA, 2009.
[46] T.H. Dunning, J. Chem. Phys. 90 (1989) 1007–1023.
[47] I. Swart, F.M.F. de Groot, B.M. Weckhuysen, D.M. Rayner, G. Meijer, A. Fielicke, J. Am. Chem. Soc. 130 (2008) 2126–2127.